Journal of Biomolecular NMR (2005) 33: 187–196
DOI 10.1007/s10858-005-3204-z

Article

Unambiguous assignment of NMR protein backbone signals with a time-shared triple-resonance experiment

Dominique P. Frueh, Haribabu Arthanari & Gerhard Wagner*
Department of Biological Chemistry and Molecular Pharmacology, Harvard Medical School, 240 Longwood Avenue, Boston, MA, 02115, USA

Received 8 August 2005; Accepted 8 September 2005

Key words: Gal11, GB1, nuclear magnetic resonance, protein backbone assignment, time-shared

Abstract

An experiment that provides a simple procedure to assign backbone nuclei in proteins is presented. The method relies on time-shared evolution of the coherences present in the (HN)NCAHA and (HA)CANNH experiments. By exploiting the fact that some of the coherences are common to both experiments the alpha and amide protons that are simultaneously detected are correlated with each other and with nitrogen and carbon nuclei. Thus, simultaneous assignment of H^{α}, H^{N}, C^{α} and N signals is achieved in a single 3D spectrum. The experiment was tested on the streptococcal protein G B1 domain (GB1) which was easily assigned using a ''stairway'' procedure and on an 11 kDa domain of the yeast transcriptional co-activator Gal11.

Introduction

Nuclear Magnetic Resonance (NMR) is now an established technique in studies of biological systems in solution. It has thus become a popular method due to its ability to provide structural, dynamic and kinetic information at an atomic level (Kay, 1998; Ferentz and Wagner, 2000; Zuiderweg, 2002). However, almost all of its applications critically depend on the ability to assign the detected signals to the nuclei present in the molecule. For protein backbone nuclei this is generally achieved by recording experiments that correlate signals belonging to successive amino acids, thus leading to a sequential assignment procedure. In particular multidimensional heteronuclear experiments have been designed in order to correlate the signals of various nuclei of the backbone atoms, via their mutual scalar couplings (Sattler et al., 1999). First, stretches of neighbouring spin-systems are identified within the spectra by comparing the chemical shifts of signals in one of the dimensions (e.g. the inter-residue signal of the C^{α} in the HNCOCA experiment with the intra-residue signal of an HNCA experiment). The signals are then tentatively attributed to individual residues by using the fact that chemical shifts are more or less characteristic for different classes of amino acids in a given structural environment. Theoretically, this can be accomplished with a single pair of triple-resonance experiments (e.g. HNCA and HNCOCA), with one experiment providing signals for a pair of adjacent residues (e.g. HNCA) and the second experiment enabling to differentiate between inter-residue and intra-residue signals (e.g. HNCOCA) (Cavanagh et al., 1996). However, in practice signal overlap leads to ambiguities in the spin system connectivity. Thus a series of multi-dimensional experiments are acquired, leading to an increase in precious measurement time. A number of techniques have been

*To whom correspondence should be addressed. E-mail: Gerhard_Wagner@hms.harvard.edu

Figure 1. Top: pulse sequence of the TS-(HA)CANH/(HN)NCAHA experiment. Narrow and wide solid rectangles indicate 90° and 180° pulses, respectively. The pulses are applied along the x axis unless specified otherwise. REBURP (Geen and Freeman, 1991) pulses (length $\tau_{REB} = 645$ μs, 12 ppm (7200 Hz) bandwidth, applied at −1 ppm) were used to selectively invert the H^{α} region. Q3 inversion pulses (256 μs, bandwidth of 88 ppm, 13.2 kHz) (Emsley and Bodenhausen, 1992) were used to affect either the on-resonance C^{α} coherences (55 ppm) or the off-resonance C′ coherences (176 ppm). The delays were: $\tau_1 = 2.4$ ms $\approx 1/(4J(\mathrm{NH}))$, $\tau_2 = 12$ms $\approx 1/(4J(\mathrm{NC}^{\alpha}))$, $\tau_3 = 5.54$ ms $\approx 1/(2J(\mathrm{NH}))$, $\delta_1 = 1.6$ ms $\approx 1/(4J(\mathrm{CH}))$, $\delta_2 = 4.0$ ms $\approx 1/(4J(\mathrm{NH})) + 1/(4J(\mathrm{CH}))$, $\delta'_2 = 3.677$ ms $= \delta_2 - \tau_{REB}/2$, $\delta_3 = 1.217$ ms $= \tau_3 - \tau_2 - \tau_{REB}/2$, $\delta_4 = 117$ μs $= \delta_3 - (\tau_g + \delta_g)$, $\delta_5 = 2.577$ ms $= \delta'_2 - (\tau_g + \delta_g)$, $\delta_6 = \tau_g + \delta_g = 1100$ μs (duration of the gradient pulse τ_g and its recovery delay, δ_g), $\Delta_1 = 780$ μs, $\Delta_2 = \Delta_1 + 2(\tau_g + \delta_g) = 2.980$ ms. Quadrature detection in t_1 and $t_1 + t'_1$ is obtained by the States-TPPI technique (Marion et al., 1989) applied to the phase ϕ_1. The time increments were $\Delta t_1 = 1/\mathrm{SW(C)}$ and $\Delta t'_1 = 1/\mathrm{SW(N)} - 1/\mathrm{SW(C)}$. The second dimension employs the gradient selection sensitivity-enhanced Echo–Antiecho method (Kay et al., 1992a, b; Palmer et al., 1991) where each value of t_2 and $t_2 + t'_2$ is recorded with (g_1, g_2, ϕ_4, ϕ_5, ϕ_6) and ($-g_1$, $-g_2$, $\phi_4 + 180$, $\phi_5 + 180$, $\phi_6 + 180$). The time increments were $\Delta t_2 = 1/\mathrm{SW(C)}$ and $\Delta t'_2 = 1/\mathrm{SW(N)} - 1/\mathrm{SW(C)}$. Proton decoupling was achieved with DIPSI (Shaka et al., 1988) decoupling with an amplitude of 3.6 kHz, while nitrogen and carbon were decoupled by using GARP decoupling (Shaka et al., 1983) with radio frequency strengths of 1.3 and 3.9 kHz, respectively. The phase cycle was $\phi_1 = 8(x), 8(-x)$, $\phi_2 = x, -x$, $\phi_3 = 4(x), 4(-x)$, $\phi_4 = 2(x), 2(-x)$, $\phi_5 = 2(-y), 2(y)$, $\phi_6 = 2(y), 2(-y)$ with the receiver $\phi_{rec} = x, -x, -x, x, -x, x, x, -x, -x, x, x, -x, x, -x, -x, x$. Sinusoidal shaped gradients were used. The gradient durations and strengths were g_0 = (1 ms, 33 G/cm), g_1 = (900 μs, −32.9 G/cm), g_2 = (900 μs, −14.8 G/cm) and g_3 = (900 μs, 4.8 G/cm). Each gradient was followed by a recovery time $\delta_g = 200$ μs. Bottom: toggling frame diagram depicting evolutions under various Hamiltonians. A change between the line labelled + and the one labelled – indicates an inversion of the Hamiltonian. A rupture in the pathways indicates a change of coherence (e.g. when a ^{15}N SQC of the H^{α} pathway is followed by a ^{15}N SQC of the H^{N} pathway). During the PEP transfer (Palmer et al., 1991; Kay et al., 1992a, b) dashed lines indicate that only part of the density operator is subject to the Hamiltonian.

proposed to accelerate the acquisition time, thus enabling more information gathering or the extension to higher dimensions (Schmieder et al., 1993; Szyperski et al., 1993; Orekhov et al., 2001; Bersch et al., 2003; Kupce and Freeman, 2003a, b; Rovnyak et al., 2004).

In this article, we present an experiment that relies on time-shared evolution of different coherences and provides additional correlations in a single spectrum, thus with no increase in acquisition time. Amide proton (H^{N}) signals are detected simultaneously with alpha protons (H^{α}) and both are correlated with nitrogen and alpha carbon coherences. In addition to common intra-residue cross-peaks, different correlations with neighbouring residues are obtained for both types of detected proton coherences. The three-dimensional experiment contains in the same spectrum the signals of $H^{N} -> N -> C^{\alpha}$ and $H^{\alpha} -> C^{\alpha} -> N$ coherence transfer pathways, with both intra- and inter-residue connectivities. After a transposition of the frequency domain data matrix, the spectrum contains complete sequence specific assignments of H^{N}, N, C^{α} and H^{α} resonances, combining the information of both an HNCA and an HNCAHA experiment. The assignment procedure relies on the fact that the two detected proton signals are correlated with each other and that a single amide proton is correlated to both inter- and intra-residue alpha *carbons*, and at the same time H^{α} protons are correlated with inter- and intra-residue *nitrogen* signals. Thus one type of proton associated with one indirect dimension provides connectivity within a plane, while the other type of proton allows making connections between planes along the second indirect dimension.

Material and methods

A plasmid pET9d containing the gene coding for the HIS-tagged GB1 protein (59 amino acid immunoglobulin binding domain from streptococcal protein G) was transformed into *E. coli* BL21(DE3) cells for protein expression. A ^{15}N/^{13}C uniformly labelled sample was prepared by overexpression in M9 minimal media containing ^{13}C glucose and $^{15}NH_4Cl$. The protein was initially purified using a Nickel resin (Qiagen). The HIS tag was later removed with TEV protease and the resulting GB1 was further purified on a FPLC using a Sephadex column. The sample was concentrated to a final concentration of 1 mM in phosphate buffer (20 mM, pH = 6.5) with 150 mM NaCl and 100 μM EDTA. The Gal11 domain (101 amino acids) was prepared using the same procedure and the sample was concentrated to 400 μM in the same buffer conditions. Over time, aggregation has been observed at concentrations higher than 400 μM.

The data were recorded at 25 °C for GB1 and at 15 °C for Gal11 on a 600 MHz Bruker

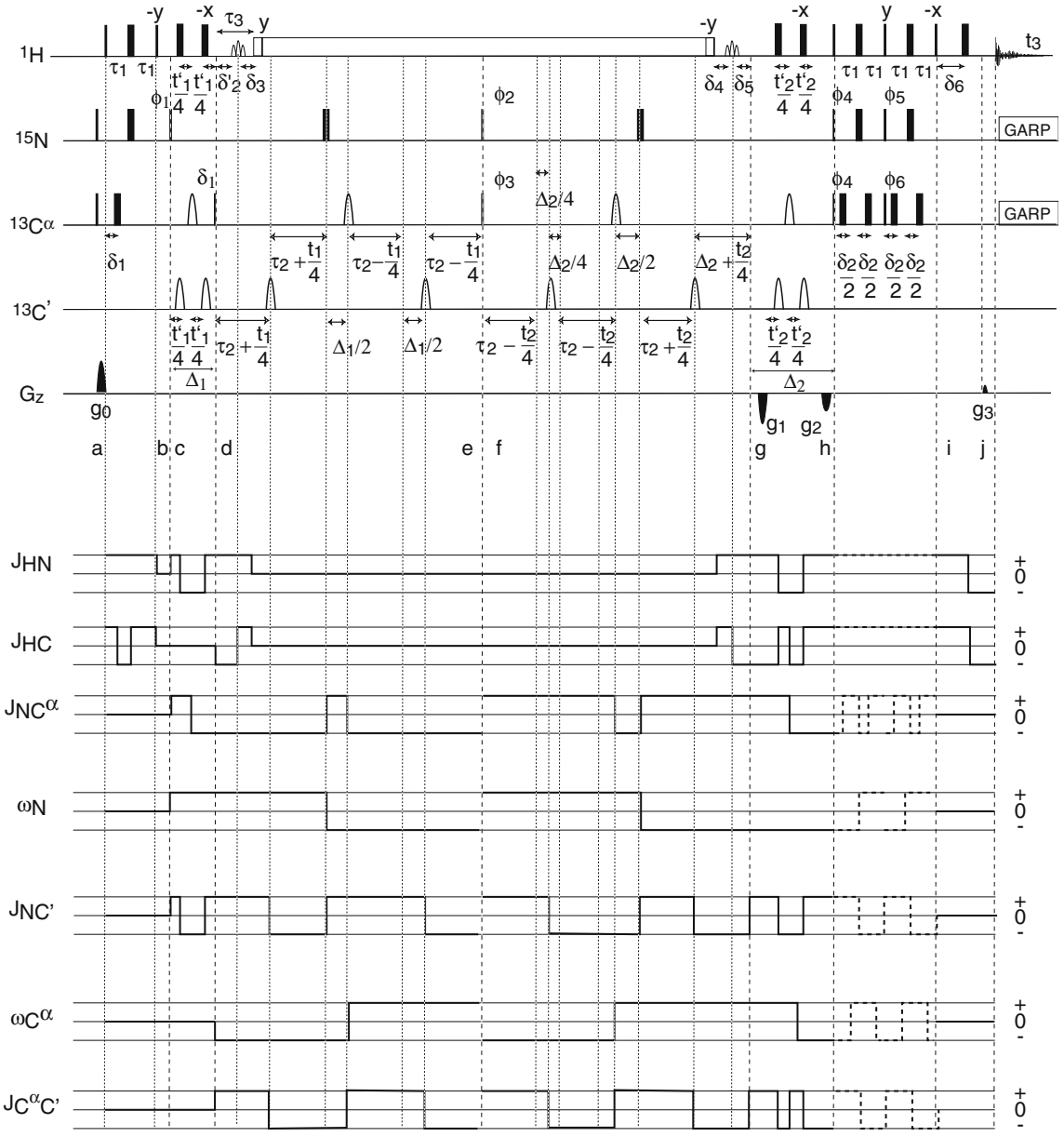

spectrometer equipped with a cryoprobe®. A data matrix of 1024 × 64 × 64 complex points was acquired for GB1, while 1024 × 43 × 43 complex points were recorded for the Gal11 domain. The spectral widths were 16 ppm for proton (centred at 4.701 ppm), 32 ppm for nitrogen (centred at 118 ppm) and 30 ppm for carbon (centred at 55 ppm). A recycling delay of 1 s was used and 16 scans were accumulated. The total measuring time was 3 days and 18 h for GB1 and 1 day and 16 h for Gal11. The spectra were extended with linear prediction to a final size of 1902 × 128 × 128 complex points. The regions between 12 and 6 ppm and between 6 and 1 ppm were extracted and the second region was transposed with respect to the two indirect dimensions. The two sub-matrices were zero-filled in the detected frequency domain to a size of 1189 complex points (11 ppm) before being added. No solvent filtration was applied during processing.

Results and discussion

Pulse sequence

The method, in effect, consists of a combination of the (H)NCAHA (Clubb et al., 1992a, b; Kay et al., 1992a, b) and (H)CANNH (Kay et al., 1991; Boucher and Laue, 1992; Clubb et al., 1992a, b) experiments, where the coherence transfers of each experiment occur simultaneously and where the two types of coherences evolve in a "time-shared" fashion (Farmer II, 1991; Pascal et al., 1994; Sattler et al., 1995; Spitzer et al., 1992).

Figure 1 shows the pulse sequence of the TS-(HA)CANH/(HN)NCAHA experiment together with a toggling frame diagram (Chiarparin et al., 1999) that indicates the alternation of the effective signs of various interactions. A first INEPT between points a and d simultaneously transfers the coherence from H^{α} to C^{α} and from H^{N} to N (Farmer II, 1991). Between c and e, ^{15}N single quantum coherence (SQC) evolves under the scalar couplings $J(NC^{\alpha})$ during $2\tau_2-\Delta_1/2 = 1/(2J(NC^{\alpha}))$ and J(NH) during $\tau_3 = 1/(2J(NH))$, and is encoded with the ^{15}N chemical shift in a semi-constant time fashion with $(t'_1 + t_1)$ (Grzesiek and Bax, 1993a; Logan et al., 1993). Similarly, between points d and e, C^{α} SQC evolves under the couplings $J(NC^{\alpha})$ and under J(CH) during $\delta'_2-\delta_3 = \delta_2-\tau_{REB}/2-(\tau_3-\delta_2-\tau_{REB}/2) = 2\delta_2-\delta_3 =$ 2.46 ms. This value is shorter than $1/2J$(CH) in order to allow for the detection of Gly residues and was optimized experimentally. During the period d–e the C^{α} SQC is encoded with the ^{13}C chemical shift in a constant time fashion with t_1. In other words, the accordion principle (Bodenhausen and Ernst, 1981; Bodenhausen and Ernst, 1982) was applied in order to match the spectral widths for both nuclei. The time increments are adjusted so that $\Delta t_1 = 1/SW(C)$ and $\Delta t'_1 = 1/SW(N) - 1/SW(C)$. As can be seen on the toggling frame diagram, all other interactions are refocused except for the small scalar coupling $J(NC')$, which is active during the short delay Δ_1 (c.a. 780 μs with the chosen pulses). The density operator σ thus evolves between points d and e as:

$$\sigma_d = 2N_{y_i}H^{N}_{z_i} + 2C^{\alpha}_{y_i}H^{\alpha}_{z_i} \longrightarrow \sigma_e = 2N_{y_i}C^{\alpha}_{z_{i-1}} + 2N_{y_i}C^{\alpha}_{z_i} + 2C^{\alpha}_{y_i}N_{z_i} + 2C^{\alpha}_{y_i}N_{z_{i+1}} \quad (1)$$

where the index i designates the residue number. At point e, the 90° radiofrequency pulses on ^{13}C and ^{15}N nuclei interconvert ^{15}N SQC and ^{13}C SQC, leading to:

$$\sigma_f = 2N_{z_i}C^{\alpha}_{y_{i-1}} + 2N_{z_i}C^{\alpha}_{y_i} + 2C^{\alpha}_{z_i}N_{y_i} + 2C^{\alpha}_{z_i}N_{y_{i+1}} \quad (2)$$

Note that, in addition to conversion of coherences occurring within a residue, the ^{15}N SQC has been converted to ^{13}C SQC of the *preceding* residue, whilst ^{13}C SQC has been converted to ^{15}N SQC of the *following* residue. Another evolution period follows between f and g, similar to the period d–e described above, where both ^{15}N and ^{13}C coherences are encoded with their respective chemical shifts. This period is followed by a real time evolution of ^{15}N SQC during which evolution under carbon chemical shift is refocused (g–h). Thus, the time increments are adjusted such that $\Delta t_2 = 1/SW(C)$ and $\Delta t'_2 = 1/SW(N) - 1/SW(C)$. Note that evolutions under the scalar coupling J(NH) and under ω(N) are effective during the two encoding gradients g_1 and g_2, whereas evolutions under J(CH) and ω(C) are refocused. Thus, the delays Δ_2,δ_4 and δ_5 differ from Δ_1, δ'_2 and δ_3 in order to readjust the evolution under J(NH) and ω(N) to 5.54 ms and 0 ms, respectively, whilst maintaining the evolution under J(CH) to 2.46 ms and the evolution under ω(C) to 0 ms (in the absence of encoding with t_2). In order to allow for a sensitivity enhanced transfer, carbon coherences are maintained during the nitrogen evolution. As a consequence, there is an additional evolution under $J(C^{\alpha}C^{\beta})$ during t'_2. However, no splitting of the lines was observed in either spectrum with the chosen resolutions. At point g, the density operator is:

$$\sigma_g = 2H^{\alpha}_{z_{i-1}}C^{\alpha}_{y_{i-1}} + 2H^{\alpha}_{z_i}C^{\alpha}_{y_i} - 2H^{N}_{z_i}N_{y_i} - 2H^{N}_{z_{i+1}}N_{y_{i+1}} \quad (3)$$

At this stage, the coherences are encoded with the gradients g_1 and g_2, between points g and h. Finally, a PEP (preservation of equivalent pathways) transfer (Palmer et al., 1991; Kay et al., 1992 a, b) converts simultaneously carbon and nitrogen coherences into proton coherences (Sattler et al., 1995) which are decoded by the gradient g_3. In order to simultaneously encode nitrogen and carbon signals, the gradients g_1, g_2 and g_3 are adjusted such that $g_1 = g_3\gamma_H(\gamma_C-\gamma_N)/\gamma_N\gamma_C \approx -7\ g_3$ and $g_2 = g_3\gamma_H(\gamma_C+\gamma_N)/\gamma_N\ \gamma_C \approx -3g_3$. One of the major reasons to use a *gradient selection* sensitivity

enhanced scheme is that the design of the pulse sequence described here relies on H^{α} detection and does not allow for the incorporation of the frequently used water flip-back (Grzesiek and Bax, 1993b) or WATERGATE (Piotto et al., 1992). The presented pulse sequence provided efficient water suppression for the two samples it was tested on.

To summarize, the coherence transfer can be described as:

$$\begin{cases} HA_i \rightarrow CA_i(t_1) \rightarrow \begin{cases} N_i(t'_2+t_2) \rightarrow HN_i(t_3) \\ N_{i+1}(t'_2+t_2) \rightarrow HN_{i+1}(t_3) \end{cases} \\ HN_i \rightarrow N_i(t'_1+t_1) \rightarrow \begin{cases} CA_i(t_2) \rightarrow HA_i(t_3) \\ CA_{i-1}(t_2) \rightarrow HA_{i-1}(t_3) \end{cases} \end{cases} \quad (4)$$

where $t'_1$and t'_2 indicate that ^{15}N single quantum coherences (SQC) evolve with a different dwell time than ^{13}C single quantum coherences. While the same type of information could be provided by a time shared evolution of the well-known HNCA (Kay et al., 1990) and HACAN (Wang et al., 1995) experiments in an out-and-back fashion, a TS-HNCA/HACAN experiment, the experiment chosen here, has the advantage of having the two coherence transfer pathways each subject to ^{15}N relaxation during one transfer period (c–e or f–h) and to ^{13}C relaxation only during the other transfer period (f–h or c–e). This avoids a dramatic loss of signals intensity for the H^{α} nuclei that would be subject to C^{α} SQC relaxation during the two transfers of the TS-HNCA/HACAN experiment. In addition, this alternate out-and-back experiment cannot benefit from the semi-constant time evolution of ^{15}N coherences and the constant time evolution of C^{α} coherences during the first evolution period and requires an additional real time evolution for both coherences.

In the two molecules for which the experiment was tested, there is no overlap between the spectral regions of amide and alpha protons. Clearly, one must record HSQC's for the two types of protons to identify eventual amide proton outliers, with frequencies in the H^{α} region. Moreover, the time-shared experiment can be designed in order to have opposite phases for the two types of protons (by inverting ϕ_1 for either carbon or nitrogen in the pulse sequence), thus unambiguously identifying them. Similarly, one must check that the shaped pulse used to invert the H^{α} region does not affect the detected signals. This can easily be achieved by replacing the REBURPs by hard inversion pulses to investigate the H^{α}, or by removing the REBURPs to monitor the H^{N}. In the rare event where a substantial amount of amide protons overlap with aliphatic protons, the "stairway" assignment procedure described below can still be applied to spectra taken separately with the (HN)NCAHA and (HA)CANNH experiments or with the HNCA and the HACAN experiments. In this case the appropriately transposed spectra must be overlaid and not summed. Note that it is critical that no shifts of frequencies occur between the two paired experiments. Thus care must be taken to avoid differential Bloch-Siegert shift effects (e.g. due to carbonyl or C^{β} decoupling). The three dimensional spectrum obtained with the presented TS-(HA)CANNH/(HN)NCAHA corresponds in effect to the superposition of the spectra of the (HN)NCAHA and (HA)CANNH experiments. Similar correlations could indeed be obtained from a 4 dimensional HCANNH (Boucher and Laue, 1992) or HNCAHA (Kay et al., 1992a, b) experiment, with the benefit of having no alpha protons hidden by the water signal, since they evolve in an indirect dimension. However this comes at the cost of a tremendous increase in experimental time and even then would provide a much lower resolution in the indirect H^{α} dimension. Due to the carefully designed water suppression scheme, our experiment has enabled us to identify all H^{α} resonances of the mixed beta-sheet and alpha-helical protein GB1, in spite of the fact that numerous H^{α} resonances are around the water signal (see also the discussion below). For Gal11, the high resolution in the detected proton dimension enabled us to unravel ambiguities resulting from spectral overlap. In contrast, the mentioned 4D experiments would not provide the sequential correlation for both protons through different coherence transfer pathways, i.e. with H^{N} correlated to C_i^{α} and C_{i-1}^{α} and H^{α} correlated to N_i and N_{i+1}, which provides a very simple assignment procedure, as described below.

Spectrum manipulation and assignment procedure

The coherences correlated in the experiment are represented graphically on Figure 2. The two

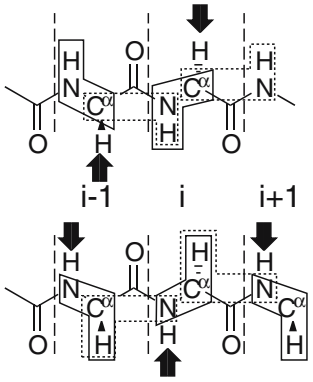

Figure 2. Coherences correlated by the TS-(HA)CANNH/(HN)NCAHA experiment. The upper panel depicts the pathways where amide protons are detected and the lower panel those where the alpha protons are detected. The frames indicate the coherences correlated with each other. Dotted frames indicate sequential correlations whereas solid frames denote intraresidue correlations. The arrows show the nuclei that are excited in the beginning of the pulse sequence.

pathways feature common coherences, therefore adding a correlation between the detected H^{α} and H^{N} signals. However, the acquired spectrum does not provide this additional information. As seen in Equation 4 and in Figure 3a, during the first evolution period amide signals are correlated with C^{α} nuclei while H^{α} signals are correlated with nitrogen. In the same way, during the second evolution period H^{N} coherences are correlated to ^{15}N coherences whereas H^{α} coherences are correlated with C^{α} nuclei (see Figure 3b). Thus, in order to take full advantage of the experiment, the indirect dimensions need to be swapped for one region in the spectrum. This can easily be achieved by extracting the two regions and transposing one of the resulting 3 dimensional matrices with respect to the two indirect dimensions. The two matrices are then summed to obtain the desired spectrum, which now features nitrogen as one indirect dimension and carbon as the second indirect dimension. A cartoon representation of reconstructing the spectrum is shown in Figure 4. The resulting projections are displayed in Figure 3c, d. To see what signals will be present in a given plane of the 3 dimensional spectrum, Equation 4 should be extended to include the pathways originating from neighbouring residues:

$$\begin{cases} \mathrm{HA}_{i-1}\rightarrow\mathrm{CA}_{i-1}(t_1)\rightarrow\begin{cases}\mathrm{N}_{i-1}(t_2'+t_2)\rightarrow\mathrm{HN}_{i-1}(t_3)\\ \mathrm{N}_{i}(t_2'+t_2)\rightarrow\mathrm{HN}_{i}(t_3)\end{cases}\\ \mathrm{HA}_{i}\rightarrow\mathrm{CA}_{i}(t_1)\rightarrow\begin{cases}\mathrm{N}_{i}(t_2'+t_2)\rightarrow\mathrm{HN}_{i}(t_3)\\ \mathrm{N}_{i+1}(t_2'+t_2)\rightarrow\mathrm{HN}_{i+1}(t_3)\end{cases}\\ \mathrm{HN}_{i}\rightarrow\mathrm{N}_{i}(t_1'+t_1)\rightarrow\begin{cases}\mathrm{CA}_{i-1}(t_2)\rightarrow\mathrm{HA}_{i-1}(t_3)\\ \mathrm{CA}_{i}(t_2)\rightarrow\mathrm{HA}_{i}(t_3)\end{cases}\\ \mathrm{HN}_{i+1}\rightarrow\mathrm{N}_{i+1}(t_1'+t_1)\rightarrow\begin{cases}\mathrm{CA}_{i}(t_2)\rightarrow\mathrm{HA}_{i}(t_3)\\ \mathrm{CA}_{i+1}(t_2)\rightarrow\mathrm{HA}_{i+1}(t_3)\end{cases}\end{cases} \quad (5)$$

Thus, after the manipulation described above, an H–C plane at the frequency $\omega(N_i)$ will contain signals correlating H_i^N with C_{i-1}^{α}, $H^{N}i$ with C_i^{α}, H_i^{α} with C^{α} and H_{i-1}^{α} with C_{i-1}^{α} (see Figure 5). The chain is easily extended by noting that the correlations between H_{i-1}^{α} and C_{i-1}^{α} are also present in a plane at the frequency $\omega(N_{i-1})$ and that the plane at $\omega(N_{i+1})$ also contains the correlation between H_i^{α} and C_i^{α}. Alternatively, H–N planes can be displayed. In this case, a plane at $\omega(C_i^{\alpha})$ features the correlations of HN_i with N_i, HN_{i+1} with N_{i+1}, H_i^{α} with N_i and H_i^{α} with N_{i+1} and the chain is extended by finding the correlation of HN_i with N_i at $\omega(C_{i-1}^{\alpha})$, or the correlation between H_{i+1}^{N} and N_{i+1} at $\omega(C_{i+1}^{\alpha})$. The four cross peaks expected for a particular spin system form an easily recognizable trapezoidal pattern with two right angles in an H–C plane, as well as in the perpendicular H–N plane of the 3D experiment. An example of such a chain extension is shown on Figure 6 for the protein GB1. A plane displaying the correlations between protons (*X* axis) and carbons (*Y* axis) is displayed at a given nitrogen frequency. Thus a single amide proton is correlated with two C^{α} frequencies, which in turn are correlated with two different alpha protons. A slice along the second indirect dimension (*Z* axis) at one of the H^{α} and C^{α} correlation peaks allows finding the plane containing the signals of the connecting residues. This ''stairway'' approach, where one finds correlations across different planes, is readily applicable for programs such as CARA (Keller, 2004) nmrView (Johnson and Blevins, 1994) or Sparky (Goddard and Kneller). The directionality of the chain can be determined by noting that the intra-residual signal of a glycine residue (with opposite phase) will appear at low frequencies in both the ^{15}N and ^{13}C dimensions, or by examining the relative intensities of the sequential signal (usually of lower

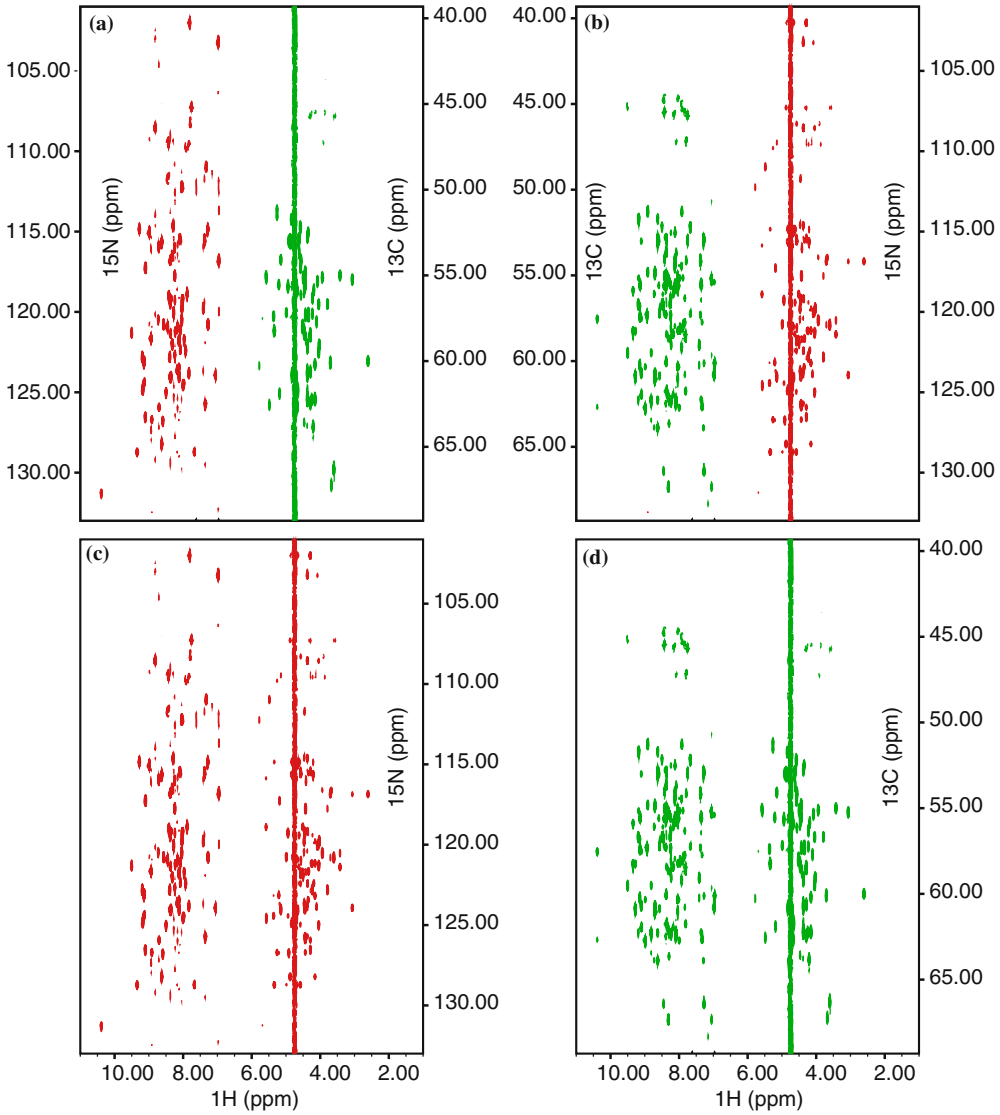

Figure 3. Projections of the TS-(HA)CANNH/(HN)NCAHA experiment recorded on GB1. (a) Projection along ω_1. The amide protons are correlated with ^{15}N coherences (red) and the alpha protons are correlated with alpha carbons (green). (b) In the projection along ω_2 the amide protons are correlated with C^{α} (green) and the alpha protons are correlated with nitrogen (red). After transposition of the two indirect dimensions for the region of the alpha protons (between 6 and 1 ppm, in this case), the two types of protons become correlated to the same nuclei in the same dimension. (c) Projection along $\omega(C^{\alpha})$, displaying H–N correlations. (d) Projection along ω(N) displaying H–C correlations. Note that correlations between the amide and alpha protons are now revealed.

intensity) and the intra-residue signal. In our example, we start by positioning the cursor on an (H^N,C^{α}) cross-peak. This allows us to identify the intra-residual signal (H_i^N, C_i^{α}, N_i) by inspecting the trace along *Y*. The corresponding (H_i^{α}, C_i^{α}, N_i) correlation is found by inspecting the trace along X. Note that this trace allows us to find the signal even in the case of strong overlap with the water signal, where the cross-peak often cannot be seen on the contour display. The cursor is moved to this correlation (indicated by a circle in Figure 6). The trace along *Z* then reveals the location of the plane of the following residue. In the program CARA, a cursor indicates the location of the current plane on the trace along *Z*. A simple click on the second peak present (which should be of smaller intensity, since we choose to start from intra-residual signals) immediately displays the next plane where

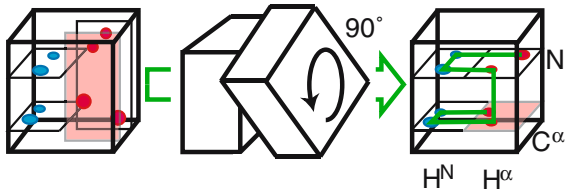

Figure 4. Cartoon representation of the data manipulation in order to reveal signal connections. Amide and alpha proton regions are separated and the latter is transposed. The two regions are then recombined.

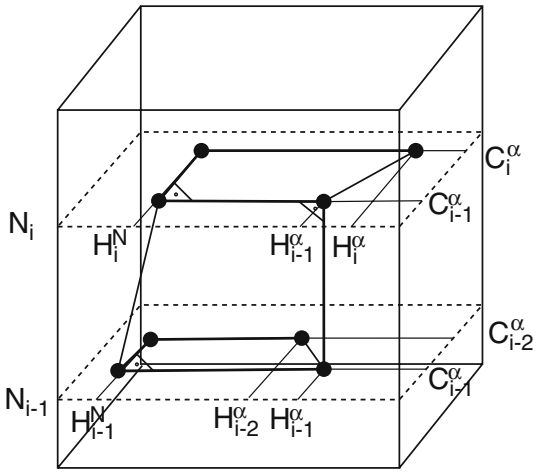

Figure 5. Schematic representation of the 3D spectrum. Each amide proton is correlated with two carbon signals whereas each alpha proton is correlated with two nitrogen signals. Sequential connections are found within a plane and between planes. Thus the identification of the connected residues is simply achieved by recognizing trapezoidal patterns within an *X*–*Y* plane (for each indirect dimension). The extension of the chain of assigned residues will occur by navigating along the second indirect dimension *Z*, going up or down the "stairways" between the signals located in different planes. The bold solid line indicates how the peaks can be used to easily extend the chain.

the correlation (H_i^{α},C_i^{α},N_{i+1}) is readily identified. The procedure is repeated, leading to simultaneous assignment of H^{α}, H^N, N and C^{α} resonances. On GB1, all signals of the 59 residues (both inter- and intra-residue and both for H^N and H^{α} pathways) where detected and the protein could easily be assigned manually in about 40 min.

To demonstrate the applicability of the method in more difficult conditions, the experiment was repeated on an 11 kDa domain of Gal11. The sample is only stable at 15 °C, at which its correlation time of 7.8 ns (calculated assuming a rigid spherical molecule) corresponds to a 15 kDa protein at 25 °C. In addition, the alpha-helical protein offers significant challenges due to a high degree of spectral overlap (see ^{15}N- and ^{13}C-edited HSQCs in the Supporting Material). Furthermore, the sample was at a concentration of 400 μM and the acquisition was restricted to a shorter time (1 day and 16 h). Given the complexity of the spectrum, a different approach was used to locate the connected peaks. Instead of displaying the H–N or H–C planes, the N–C planes containing the connectivities between residues are shown. Figure 7 shows an example of a chain extension. Planes correlating nitrogen (*X* axis) with carbons (*Y* axis) are displayed. When the plane is shown at the position of amide protons (along *Z*),as for H^N 46, the (H_i, C_i^{α}, N_i) and (H^N, C_{i-1}^{α}, N_i) signals can be identified. A slice along *Z* on (H_i^N, C_i^{α}, N_i) will reveal the H^{α} of residue 46. By moving the plane along the *Z* axis to the position of this H^{α}, the connection between (H_i^{α}, C_i^{α}, N_i) and (H^{α}, C_i^{α}, N_{i+1}) can be found. A slice along *Z* on the latter signal then enables to identify the amide proton of residue 47. When the plane is moved to the corresponding chemical shift along *Z*, the C^{α} and thus the corresponding H^{α} are both readily identified. Under our experimental conditions 11% of the H^{α} signals were missing, or were too ambiguous to allow an easy chain extension. However, the corresponding residues could still be connected via strip comparisons. The remaining of the protein could be assigned by using the stairway procedure. Thus, all 100 residues of the Gal11 domain could be assigned with a single experiment. This includes two prolines whose H^{α} could readily be assigned from the subsequent residues. The result was then confirmed by an independent conventional assignment using the HNCA, HNCOCA, HNCOCACB, HNCACB, HNCO and HNCACO spectra. However, 9 residues could only be assigned by using the TS-(HA)CANH/(HN)NCAHA experiment due to extensive overlap which could only be alleviated with the additional H^{α} correlation. Furthermore, one peak was incorrectly assigned by using only the conventional approach.

Conclusion

By designing an experiment that provides the information contained in the two experiments (HA)CANNH and (HN)CAHA simultaneously, we developed a new assignment strategy that is both faster than usual strip comparison and

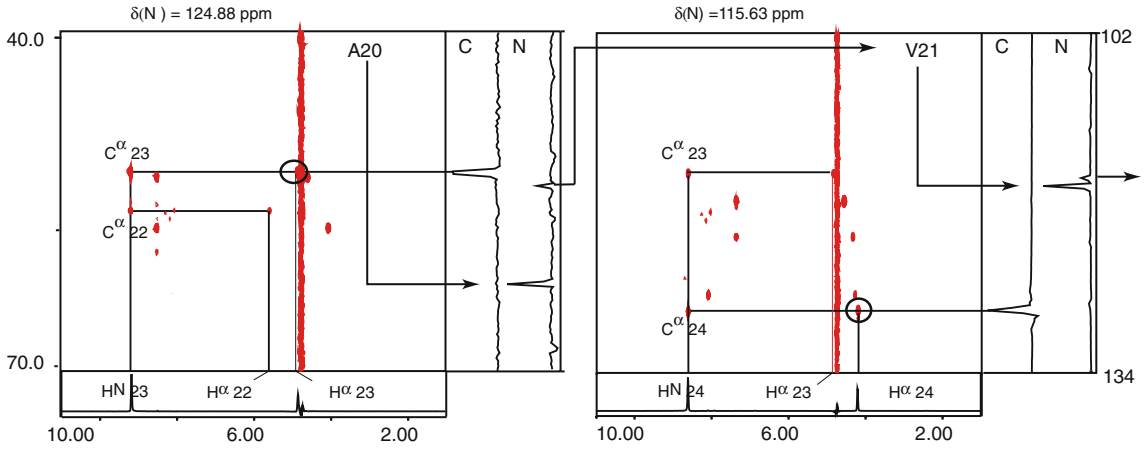

Figure 6. Sequential assignment using the "stairway" procedure on GB1. The planes display H–C$^{\alpha}$ correlations at $\omega(N_i)$, where an H^N signal is correlated to C_i^{α} and C_{i-1}^{α} coherences. Each of these carbons is correlated with a different H^{α} proton, which themselves are correlated each to different nitrogen, N_{i-1} or N_{i+1} respectively. For each plane, cross-sections are shown for one of the signals connecting two different planes. The connection to the next plane at $\omega(N_{i+1})$ is achieved via the cross-section along the nitrogen dimension (second vertical cross-section for each plane) of one of these H^{α}-C^{α} correlation. In our example, we choose to use the intra-residual cross-peak, thus extending the chain with increasing residue numbers.

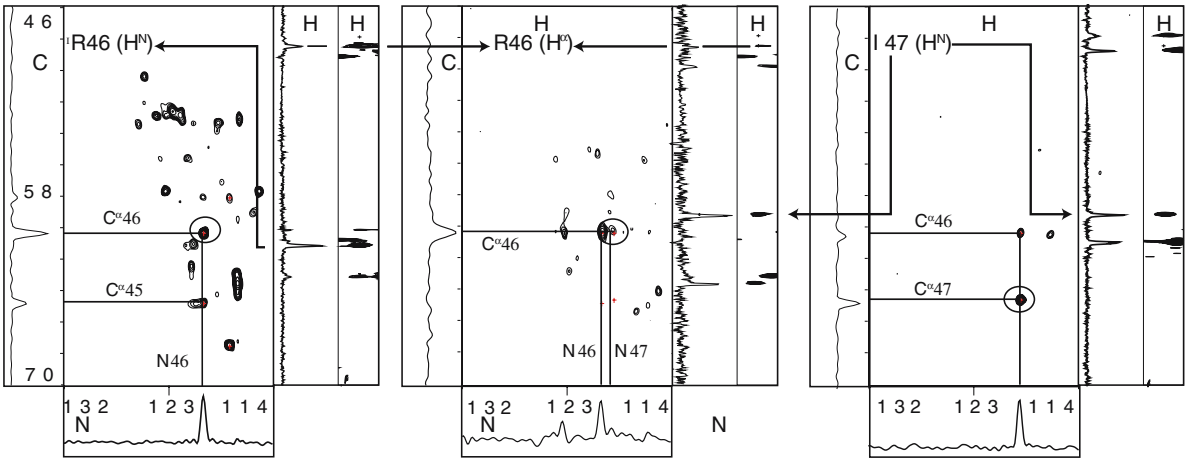

Figure 7. Sequential assignment using the "stairway" procedure on the Gal11 domain. The N–C planes are located alternatively at the frequencies of amide or alpha protons. The labels R 46 (H^N), R 46 (H^{α}) and I 47 (H^N) indicate the positions of the N–C planes in the proton dimension. These protons are displayed in the vertical axis in the C–H strips at the right of the corresponding plane, as well as in a slice along the same dimension. The circles indicate the peaks corresponding to the slices displayed for each dimension. Each plane surrounded by the slices and the strips corresponds to the display in "polyscope" in the program CARA, where an additional N–H strip is displayed.

resolves possible ambiguities. Recognition of trapezoidal patterns of cross peaks is much easier and less prone to error than matching chemical shifts between strips of different triple-resonance experiments. This avoids mismatches due to spectral changes caused by spectrometer instabilities. Moreover, the experiment obtains the information of two triple-resonance experiments within the time of one. The experiment has been designed in order to feature optimum water suppression without affecting the nearby signals of H^{α} nuclei. The frequency encoding periods that lead to the desired correlations have been tailored in order to provide familiar three dimensional spectra, thus eliminating the need to account for aliased signals.

For small proteins with good dispersion in the NMR spectra, it can be used as a means to rapidly assign H^{α}, C^{α}, H^N and N resonances by using a

"stairway" procedure, where correlations can be found within a plane and between planes of the spectrum. For more crowded spectra, such as for alpha-helical proteins, the technique alleviates spectral overlap issues by adding new correlated signals in the detected dimension. In case of total degeneracy between the resonance of an alpha proton and the one of the water signal, the experiment can be used in the same way as a traditional HNCA, by using strip comparison. For large molecules, the experiment requires substantial modifications and is currently under investigation. The pulse sequence of the TS-(HA)CANH/(HN)NCAHA experiment, as well as the accompanying nmr Pipe processing script, can be downloaded at http://gwagner.med.harvard.edu.

Acknowledgments

We thank Dr. Philipp Selenko for providing the GB1 construct and Anders M. Näär for the gene of the Gal11 domain. This research was supported by NIH (grants GM 47467 and RR 00995).

References

Bersch, B., Rossy, E., Coves, J. and Brutscher, B. (2003) *J. Biomol. NMR*, **27**, 57–67.
Bodenhausen, G. and Ernst, R. (1981) *J. Magn. Reson.*, **45**, 319 .
Bodenhausen, G. and Ernst, R. (1982) *J. Am. Chem. Soc.*, **104**, 1304–1309.
Boucher, W. and Laue, E. (1992) *J. Am. Chem. Soc.*, **114**, 2262–2264.
Cavanagh, J., Fairbrother, W.J., Palmer, A.G. and Skelton, N.J. (1996) *Protein NMR Spectroscopy Principles and Practice*, Academic Press, San Diego.
Chiarparin, E., Pelupessy, P., Ghose, R. and Bodenhausen, G. (1999) *J. Am. Chem. Soc.*, **121**, 6876–6883.
Clubb, R., Thanabal, V. and Wagner, G. (1992a) *J. Magn. Reson.*, **97**, 213 .
Clubb, R., Thanabal, V. and Wagner, G. (1992b) *J. Biomol. NMR*, **2**, 203–210.
Emsley, L. and Bodenhausen, G. (1992) *J. Magn. Reson.*, **97**, 135–148.
Farmer II, B. (1991) *J. Magn. Reson.*, **93**, 635–641.
Ferentz, A.E. and Wagner, G. (2000) *Q. Rev. Biophys.*, **33**, 29–65.
Geen, H. and Freeman, R. (1991) *J. Magn. Reson.*, **93**, 93–141.
Goddard, T.D. and Kneller, D.G. (2004) SPARKY 3, University of California, San Fransisco.
Grzesiek, S. and Bax, A. (1993a) *J. Biomol. NMR*, **3**, 185–204.
Grzesiek, S. and Bax, A. (1993b) *J. Am. Chem. Soc.*, **115**, 12593–12594.
Johnson, B.A. and Blevins, R.A. (1994) *J. Biomol. NMR*, **4**, 603–614.
Kay, L., Ikura, M. and Bax, A. (1991) *J. Magn. Reson.*, **91**, 84–92.
Kay, L.E. (1998) *Nat. Struct. Biol.*, **5 Suppl**, 513–7.
Kay, L.E., Ikura, M., Tschudin, R. and Bax, A. (1990) *J. Magn. Reson.*, **89**, 496–514.
Kay, L., Wittekind, M., McCoy, M., Friedrichs, M. and Mueller, L. (1992a) *J. Magn. Reson.*, **98**, 443–450.
Kay, L.E., Keifer, P. and Saarinen, T. (1992b) *J. Am. Chem. Soc.*, **114**, 10663–10665.
Keller R. (2004) CANTINA verlag, Goldau.
Kupce, E. and Freeman, R. (2003a) *J. Am. Chem. Soc.*, **125**, 13958–13959.
Kupce, E. and Freeman, R. (2003b) *J. Magn. Reson.*, **162**, 300–10.
Logan, T.M., Olejniczak, E.T., Xu, R.X. and Fesik, S.W. (1993) *J. Biomol. NMR*, **3**, 225–231.
Marion, D., Ikura, M., Tschudin, R. and Bax, A. (1989) *J. Magn. Reson.*, **85**, 393–399.
Orekhov, V.Y., Ibraghimov, I.V. and Billeter, M. (2001) *J. Biomol. NMR*, **20**, 49–60.
Palmer, A.G., Cavanagh, J., Wright, P.E. and Rance, M. (1991) *J. Magn. Reson.*, **93**, 151–170.
Pascal, S., Muhandiram, D., Yamazaki, T., Forman-Kay, J. and Kay, L. (1994) *J. Magn. Reson. Ser. B*, **103**, 197–201.
Piotto, M., Saudek, V. and Sklenar, V. (1992) *J. Biomol. NMR*, **2**, 661–665.
Rovnyak, D., Frueh, D.P., Sastry, M., Sun, Z.Y., Stern, A.S., Hoch, J.C. and Wagner, G. (2004) *J. Magn. Reson.*, **170**, 15–21.
Sattler, M., Maurer, M., Schleucher, J. and Griesinger, C. (1995) *J. Biomol. NMR*, **5**, 97–102.
Sattler, M., Schleucher, J. and Griesinger, C. (1999) *Progr. NMR Spectrosc.*, **34**, 93–158.
Schmieder, P., Stern, A.S., Wagner, G. and Hoch, J.C. (1993) *J. Biomol. NMR*, **3**, 569–56.
Shaka, A.J., Barker, P. and Freeman, R. (1983) *J. Magn. Reson.*, **51**, 547 .
Shaka, A.J., Lee, C.J. and Pines, A. (1988) *J. Magn. Reson.*, **77**, 274–293.
Spitzer, T., Martin, G., Crouch, R., Shockor, J. and Farmer, B. II (1992) *J. Magn. Reson.*, **99**, 433–438.
Szyperski, T., Wider, G., Bushweller, J.H. and Wuthrich, K. (1993) *J. Biomol. NMR*, **3**, 127–132.
Wang, A., Grzesiek, S., Tschudin, S., Lodi, R. and Bax, A. (1995) *J. Biomol. NMR*, **5**, 376–382.
Zuiderweg, E.R. (2002) *Biochem.*, **41**, 1–7.